Interface control of surface photochemical reactivity in ultrathin epitaxial ferroelectric films

Jason Chen, Haidong Lu, Heng-Jui Liu, Ying-Hao Chu, Steve Dunn, Kostya (Ken) Ostrikov, Alexei Gruverman, and Nagarajan Valanoor

Articles you may be interested in

Epitaxial ferroelectric BiFeO3 thin films for unassisted photocatalytic water splitting
Appl. Phys. Lett. 103, 062901 (2013); 10.1063/1.4817907

Electrode interface control of the Schottky diode-like behavior in epitaxial Pb(Zr0.2Ti0.8)O3 thin films: A critical analysis
J. Appl. Phys. 113, 214108 (2013); 10.1063/1.4808464

Role of dual-laser ablation in controlling the Pb depletion in epitaxial growth of Pb(Zr0.52Ti0.48)O3 thin films with enhanced surface quality and ferroelectric properties
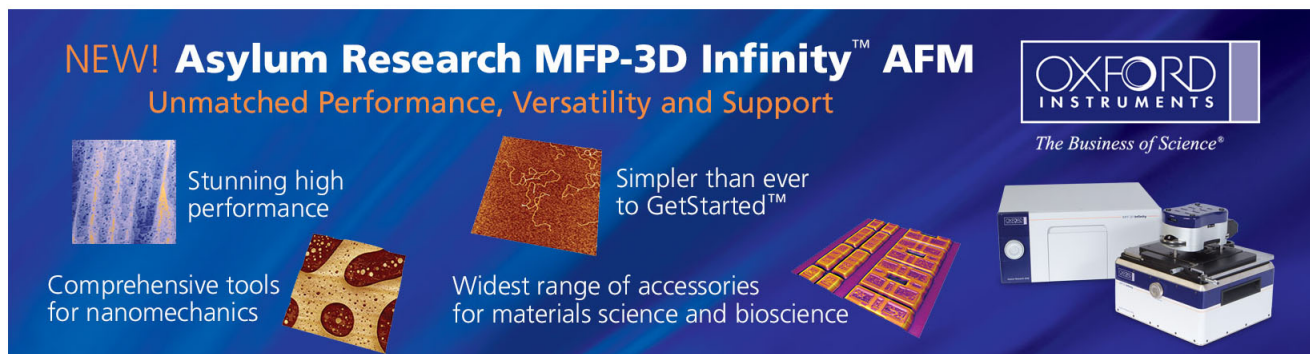J. Appl. Phys. 111, 064102 (2012); 10.1063/1.3694035

Epilayer control of photodeposited materials during UV photocatalysis
Appl. Phys. Lett. 94, 232901 (2009); 10.1063/1.3151820

The influence of the top-contact metal on the ferroelectric properties of epitaxial ferroelectric Pb (Zr 0.2 Ti 0.8) O 3 thin films
J. Appl. Phys. 104, 114101 (2008); 10.1063/1.3021293

Interface control of surface photochemical reactivity in ultrathin epitaxial ferroelectric films

Jason Chen,[1,2] Haidong Lu,[3] Heng-Jui Liu,[4] Ying-Hao Chu,[4] Steve Dunn,[5] Kostya (Ken) Ostrikov,[2,6] Alexei Gruverman,[3] and Nagarajan Valanoor[1,a]

[1]*School of Materials Science and Engineering, University of New South Wales, Sydney, New South Wales 2052, Australia*
[2]*CSIRO Materials Science and Engineering, P.O. Box 218, Lindfield, New South Wales 2070, Australia*
[3]*Department of Physics and Astronomy, University of Nebraska Lincoln, Lincoln, Nebraska 68588, USA*
[4]*Department of Materials Science and Engineering, National Chiao Tung University, Hsinchu, Taiwan*
[5]*School of Engineering and Materials, Queen Mary University of London, Mile End Road, E1 4NS London, United Kingdom*
[6]*School of Physics, The University of Sydney, Sydney, New South Wales 2006, Australia*

Asymmetrical electrical boundary conditions in (001)-oriented $Pb(Zr_{0.2}TiO_{0.8})O_3$ (PZT) epitaxial ultrathin ferroelectric films are exploited to control surface photochemical reactivity determined by the sign of the surface polarization charge. It is shown that the preferential orientation of polarization in the as-grown PZT layer can be manipulated by choosing an appropriate type of bottom electrode material. PZT films deposited on the $SrRuO_3$ electrodes exhibit preferential upward polarization (C^+) whilst the same films grown on the $(La,Sr)CoO_3$-electrodes are polarized downward (C^-). Photochemical activity of the PZT surfaces with different surface polarization charges has been tested by studying deposition of silver nanoparticles from $AgNO_3$ solution under UV irradiation. PZT surfaces with preferential C^+ orientation possess a more active surface for metal reduction than their C^- counterparts, evidenced by large differences in the concentration of deposited silver nanoparticles. This effect is attributed to band bending at the bottom interface which varies depending on the difference in work functions of PZT and electrode materials. © 2013 AIP Publishing LLC. [http://dx.doi.org/10.1063/1.4802885]

Ferroelectric nanolithography is a versatile fabrication technique, which exploits the polarization-dependent photochemical reactivity of ferroelectric surfaces.[1,2] The underpinning mechanism of ferroelectric nanolithography is a surface band bending determined by polarization orientation, which creates different degrees of Stern layer formation, and hence, differences in the local surface reactivity.[2,3] Previous studies have established that C^+ domains (with upward, or away from the substrate polarization) are more photochemically active than C^- (downward polarized) domains.[4,5] Photochemical reactivity has been exploited to achieve domain-specific surface decoration by metallic nanoparticles through ion reduction from the corresponding aqueous salt solution.[6,7] In the past few years, complex multi-component devices have been fabricated by attaching diverse groups of molecules on metallic nanoparticle templates synthesized by ferroelectric nanolithography.[8–10]

In spite of this progress, efforts so far have mostly focused on relatively thick (hundreds of nanometers or several micrometers) ferroelectric films, where randomly distributed polarization makes reliable control of photochemical activity difficult.[2] However, the ability to fabricate preferentially polarized ultrathin films offers an opportunity for the selective creation of photochemically reactive and passive surfaces without the need for sequential biasing of the ferroelectric film. In such a system, an active as-grown (or virgin) state can be utilized as a template for the growth of high-density nanoparticles. The overall benefits of using as-grown samples include a shorter fabrication time, reduced possibility of dielectric breakdown during poling, and a more homogeneously polarized surface.

In this work, we exploit the interdependency between the electronic carrier type in the bottom electrode and its influence on the polarization direction in an ultrathin ($\sim 10\,nm$) epitaxial ferroelectric layer to achieve direct control of the surface photochemical reactivity. We employ ultra-thin films since a significant volume fraction of these films is under depletion or accumulation conditions as a result of strong band-bending at the top and bottom interfaces.[5] In this work, the choice of bottom electrode material (either p-type $La_{0.5}Sr_{0.5}CoO_3$ (LSCO) or n-type $SrRuO_3$ (SRO)) provides the driving force to determine the preferential downward (on the LSCO electrode) or upward (on the SRO electrode) polarization orientation of the $Pb(Zr_{0.2}TiO_{0.8})O_3$ (PZT) film. This approach has been previously exploited to achieve self-polarized as-grown ferroelectric thin films for pyroelectric applications.[11] We found that PZT films grown on SRO (with preferential C^+ orientation) possess a more active surface for metal reduction than C^- counterparts (grown on LSCO). This was evidenced by a large difference in the concentration of silver (Ag) nanoparticles deposited under UV irradiation on the two surfaces. A thicker PZT film (120 nm) demonstrated a lower concentration of Ag nanoparticles under the same illumination conditions. We rationalize our findings based on a band structure model, where the low thickness of the C^+ film is shown to dramatically increase the availability of

a)nagarajan@unsw.edu.au

subsurface electrons under UV illumination, thus, improving penetrability of the ferroelectric barrier.[5,12,13]

Epitaxial (001) PZT films were deposited on (001) stepped SrTiO₃ (STO) substrates (Shinkosa Co Ltd, Japan) buffered with either SRO or LSCO electrodes in ambient oxygen pressures ranging from 45 mTorr to 100 mTorr by pulsed laser deposition (PLD) system. The substrate-target distance was fixed at 15 cm with fluence ranging from 2 to 2.5 J cm^{-2} at a laser repetition rate of 10 Hz. The films were quenched at 20 °C/min to room temperature in 450 Torr of oxygen partial pressure. Growth rate for all films was found to be 2 nm/1000 pulses. Reciprocal space maps (RSMs) of PZT (203) reflections were performed using a synchrotron radiation source with 12 keV at beamline BL-13 A at the National Synchrotron Radiation Research Center (NSRRC) in Hsinchu, Taiwan, to confirm epitaxial quality. The incident beam was monochromated with a Si (111) double crystal mirror and then focused by a vertically focusing mirror to increase beam intensity. Two sets of slits were placed before samples to attain a beam spot of approximately 0.2 mm × 0.8 mm. A second pair of slits was placed behind the sample to reduce background noise. Surface topography and polarization imaging were performed using a commercial Atomic Force Microscope (AFM) system (MFP-3D, Asylum Research). Dual AC resonance tracking (DART) mode of piezoresponse force microscopy (PFM)[14] was employed for domain visualization and hysteresis loop measurements using an ac bias of 0.4 V at 300 kHz applied to the tip. For the photoreduction experiments, a 0.1M AgNO₃ solution was prepared by dissolving appropriate amounts of AgNO₃ powder into deionized water. A drop of freshly prepared solution was placed onto the PZT surface before being irradiated with 5000 pulses of KrF laser beam (150 mJ/cm^{-2}) at 10 Hz (Lambda Physik). The laser beam was unfocussed to ensure the physical integrity of the film is maintained. The samples were then rinsed in deionized water and blown dry with nitrogen gas. Scanning electron microscopy (SEM) and X-ray energy dispersion spectroscopy (EDX) were performed using a FEI Nova NanoSEM 230 FESEM for surface morphology and chemical analysis after UV-irradiation.

Strongly tetragonal PZT (001) epitaxial films were chosen for this study. When deposited on STO, the PZT lattice is under in-plane compression imposed by the smaller STO lattice further stabilizing the c-axis and giving robust polarization values.[15] We used 10-nm-thick PZT films because at this thickness, the films are thick enough not to be affected by thickness-scaling effects,[16] yet thin enough so that sub-surface band bending at top and bottom interfaces becomes important.[5,17]

Figures 1(a) and 1(b) illustrate the two heterostructure systems studied in this paper. Synchrotron X-ray $\theta - 2\theta$ diffraction, RSM, and AFM investigations confirmed that the films were fully c-axis oriented and showed high-quality step-flow layer-by-layer growth [see supplementary material S1 and S2 for synchrotron data[24]]. To probe the virgin polarization state of the films and film-switchability, PFM poling and imaging of bi-domain patterns was performed in several surface locations (Figs. 2(a) and 2(c)). It can be seen that the as-grown film area outside of the poled regions exhibits uniform contrast which is opposite for the two samples. The images show no 180° domains within the resolution (∼10 nm) of the PFM. This observation suggests that changing from the p-type (LSCO) to the n-type (SRO) bottom electrode results in opposite preferential polarization of the PZT films.

PFM hysteresis loop measurements were performed to probe the direction of the built-in electric field that has caused the observed significant level of net polarization.[18] Figures 2(b) and 2(d) show a horizontal shift in the PFM hysteresis loops in both samples. The positive (negative) shift in the PFM loop of the PZT/SRO/STO (PZT/LSCO/STO) sample is an evidence of an upward (downward) oriented internal electric field. The direction of the internal fields in two samples is in line with the virgin state polarization direction inferred from the PFM imaging experiments. From the magnitude of the horizontal shift, we have found that the internal field is approximately five times higher in PZT/LSCO/STO (500 kV/cm) than for PZT/SRO/STO (100 kV/cm). Thus, there is a direct correlation between the bottom electrode material and the resulting polarization direction. This offers a useful tool to create photochemically active or passive ferroelectric surfaces simply based on choice of the bottom electrode.

We now turn our attention to the photochemical reduction experiment results. The KrF laser used for photoexcitation has a wavelength of 248 nm, equivalent to an incident energy of 5.03 eV, which is much larger than the bandgap of PZT (3.5 eV). Photons with the band gap energy would cause electron/hole pair formation only if they were absorbed by the ferroelectric. However, density-of-states calculations show that absorption of photons by PZT is weak around the band gap. In order to generate sufficient amount of electron/hole pairs, photons with super-bandgap energy are required, necessitating the use of the KrF laser. These high-energy photons generate photocarriers that participate in the redox reactions at the surface. At this energy level, Ag particle formation will precipitate in both the C$^-$ and C$^+$ domains.[5]

Photo-induced nucleation and growth of Ag nanoparticles on the PZT surface are illustrated by Figures 3(a), 3(b), 3(d), and 3(e) showing AFM and SEM images of PZT/SRO/
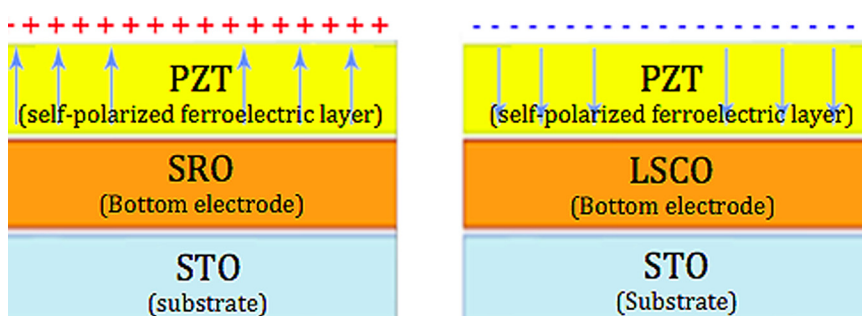

FIG. 1. Schematic illustrations of the heterostructures investigated in this study showing the preferential polarization orientation induced by SRO and LSCO bottom electrodes.
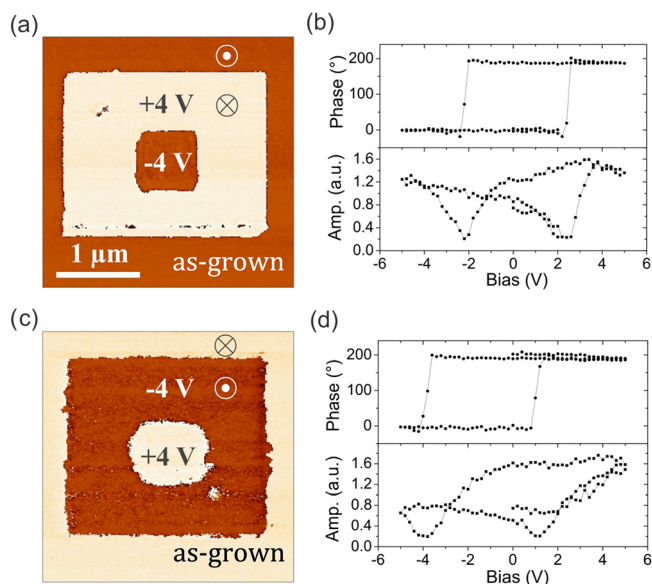
FIG. 2. PFM phase images ((a) and (c)) and local PFM hysteresis loops ((b) and (d)) acquired in PZT/SRO/STO ((a) and (b)) and PZT/LSCO/STO ((c) and (d)) heterostructures. $2 \times 2\ \mu m^2$ and $0.5 \times 0.5\ \mu m^2$ domains were written in the virgin films by applying a dc bias of ± 4 V to the tip. The PFM images indicate a positive preferentially polarized virgin state in PZT/SRO/STO and negative preferentially polarized virgin state in PZT/LSCO/STO. This is consistent with the opposite imprint in these heterostructures revealed by the hysteresis loops.

STO and PZT/LSCO/STO samples before and after UV exposure. The density of the nanoparticles is higher on PZT/SRO/STO than on PZT/LSCO/STO ($432\ \mu m^{-2}$ vs $208\ \mu m^{-2}$, respectively) [see supplementary material S3 for particle size distribution]. This is consistent with the previous studies.[2,3] Figures 3(c) and 3(f) are the EDX scans which confirm the presence of silver on the PZT and indicate that the signal intensity correlates directly with the density of particulate formations observed on PZT/SRO/STO and PZT/LSCO/STO.

To understand the mechanism behind the observed differences in deposition of silver on PZT, we first consider if the primary mechanism driving these charges is the temperature change due to the varying optical absorption

characteristics for each kind of bottom electrode. First, the reported optical absorption length for PZT at 248 nm illumination is 26 nm.[19] This exceeds the 10 nm thickness of PZT films used here. However, it can be estimated that ~60%–80% of energy will be absorbed by the PZT layers in both cases. Any light that is not absorbed by the PZT will penetrate the electrodes and reach the STO substrate, where it will be absorbed [see plot in supplementary material S4].

The thermal diffusion length for a similar perovskite material, $(Pb_{0.90}La_{0.07})(Zr_{0.5}Ti_{0.5})O_3$ (PLZT), has been reported to be 125 nm.[19] This length greatly exceeds the thickness of the PZT films studied here. Given that this thermal diffusion length is relatively large in comparison to the PZT thickness, the surface of the PZT is expected to heat at a very similar rate for all samples studied. This would be so, even after allowing for generous differences in the thermal diffusion coefficient between the reported PLZT and PZT. In other words, any photon absorption that caused heating will lie in a region that is within the thermal diffusion length of the PZT thus generating similar heating (and related effects) for both electrode systems. Furthermore, numerical calculations based on the model of Bharadwaja *et al.*,[20] were carried out in order to the estimate the temperature rise due to photon absorption. These are given in the supplementary section. We find that the increase in temperature is negligible [see supplementary material S4]. Therefore, we conclude that a temperature change between the two different systems is not the driving mechanism for the observed differences.

Instead, it is proposed that the observed differences can be attributed to the difference in band bending at the bottom interfaces. Such a case has been proposed for the case of photochemical reactivity of ultra-thin titania films on $BaTiO_3$ substrates.[21] Ferroelectric materials can be considered as wide bandgap semiconductors that exhibit a spontaneous polarization.[22] At a ferroelectric surface where the continuity of a domain is terminated, the spontaneous polarization creates a surface bound charge (or surface polarization charge) $\sigma = P \cdot n$, where P is the polarization vector and n is a unit normal to the surface. The surface polarization charge causes band bending within a subsurface region termed the space
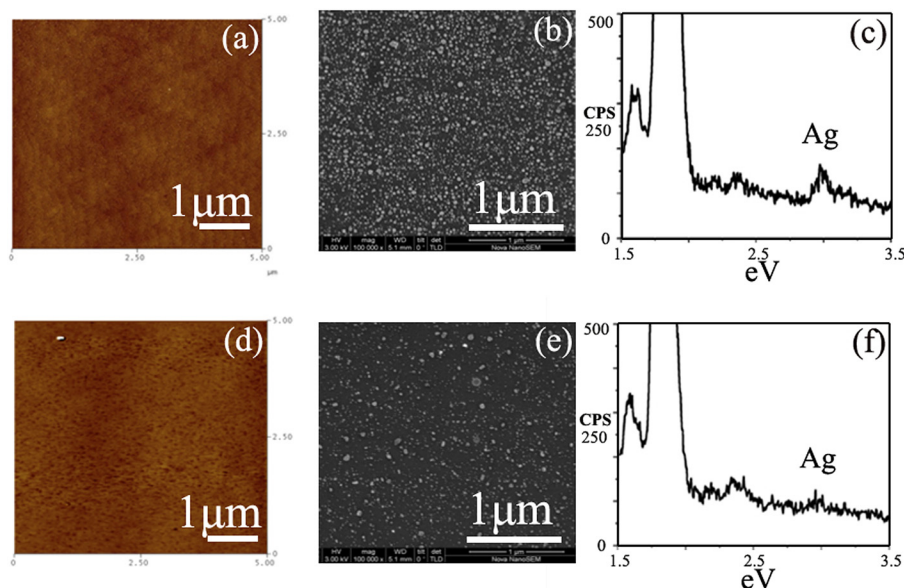

FIG. 3. AFM ((a) and (d)), SEM ((b) and (e)) and EDX ((c) and (f)) data acquired in PZT/SRO/STO ((a)–(c)) and PZT/LSCO/STO ((d)–(f)). AFM images show clean sample surfaces without any particles before UV irradiation. The SEM images obtained after UV irradiation show the appearance of particulates with the particle density being visibly higher on PZT/SRO/STO. EDX scans confirm the presence of Ag on both samples after UV irradiation with the intensity of the Ag signal being more prominent in PZT/SRO/STO.

charge region (SCR) associated with an electric field gradient. As the length scale of the ferroelectric thickness is of the same order as the space charge layer, the influence of the band bending at the bottom interface can no longer be ignored. The photochemical behaviour of the ferroelectric is now strongly influenced by the internal electric field gradient stemming from the band bending. To demonstrate the significance of the reduced film thickness and the resultant subsurface band bending, we have developed a series of band diagrams showing the progression of band bending under charge accumulation and Stern layer formation.

Figures 4(a)–4(d) are the proposed band diagrams for the heterostructures studied in this work. The initial band profiles are approximated as slanted slopes with no flat-band region as the oppositely bent bands from top and bottom interfaces overlap for such a small length scale (Figure 4(a)). The implication of such a band structure is that a significant proportion of electron/hole pairs generated under illumination will be separated and swept towards their respective interfaces where they will accumulate. Figure 4(b) shows that free electrons generated in PZT/SRO/STO heterostructure will drift towards the film top surface whilst the positive holes will migrate to the bottom interface.
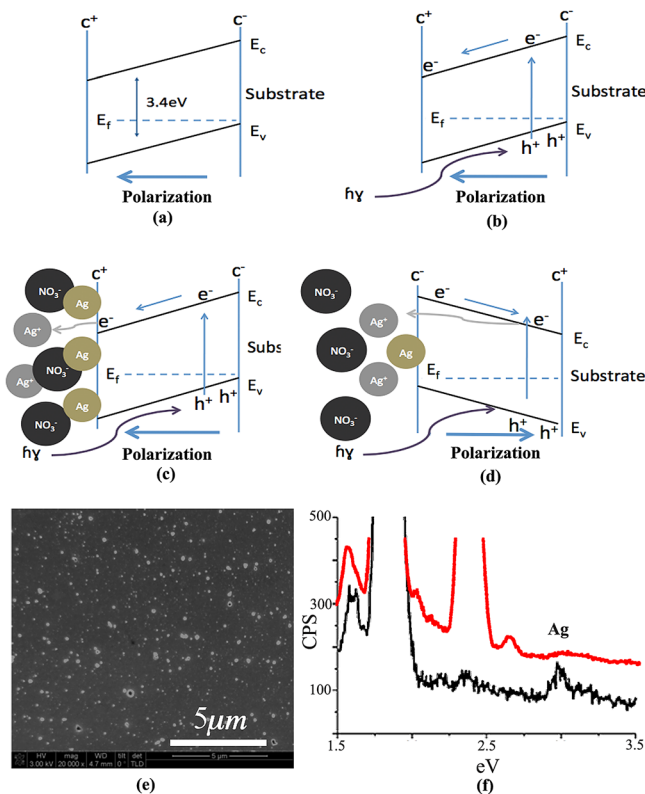

FIG. 4. Band diagrams for 10 nm PZT thin films showing fully slanted band structures without any flat-band region as the film thickness is within the same length scale as the screen charge region. (a)–(c) are band diagrams for a positive preferentially polarized PZT thin film that show the respective drift direction of electrons and holes within such a band structure; the accumulation of electrons under film surface in this case allows the reduction of Ag ions to occur more readily. (d) The band structure is sloped in the opposite direction for a negative preferentially polarized PZT, which causes the electrons to travel into the bulk of the film. (e) SEM for 120 nm PZT after UV irradiation showing precipitation of Ag particles. (f) In the EDX measurement, the Ag signal from the 120 nm PZT (red) is much weaker than the 10 nm PZT (black).

This increase in subsurface electrons will help de-pin the negatively charged NO_3^- ions at the PZT surface (Figure 4(c)) allowing electrons and Ag^+ ions to come into direct contact for photochemical reduction. Conversely, for negative preferentially polarized PZT/LSCO/STO (Figure 4(d)), the oppositely slanted band in PZT/LSCO/STO causes electrons to drift into the bulk and positive holes to accumulate at the top ferroelectric/air interface. The accumulation of electrons at the bottom interface would flatten the bottom segment of the SCR, reducing electron drift towards the bottom and increasing the diffusion current of electrons towards the top surface.

The change in the Stern layer (and electron accumulation) that occurs when the PZT is illuminated leads to a reduction in physical separation between photogenerated electrons and Ag+ ions on the surface and changes the penetrability, T, of the barrier[23]

$$\frac{T_1}{T_2} = \exp(2\alpha\Delta w), \quad (1)$$

$$\alpha = \frac{1}{\hbar}\sqrt{2mE}, \quad (2)$$

where Δw is the change in distance between electrons and the interface with the chemisorbed Ag^+, $\hbar$ is the angular momentum, m is the electron mass, and E is the potential barrier height.

As is shown in Figure 4, there exists an energy barrier between electrons and metal ions in the solution, which prevents the initiation of the reduction reaction and deposition of silver. However, this energy barrier can be overcome if the concentration of free carriers within the PZT is increased. This underlines the importance of using the shorter UV wavelength.

The band diagrams in Figure 4 show that at the onset of the chemical reaction, there is no significant barrier between the electrons in the conduction band of the PZT and Ag^+ ions in solution for the PZT/SRO/STO system. While in PZT/LSCO/STO, there exists a non-vanishing depletion region. This difference in band structures manifests itself in larger as well as higher Ag nanoparticles density for the upwardly polarized PZT/SRO/STO.

To test the validity of the proposed band structure model, a thicker (120 nm) fully c-axis oriented PZT film on SRO/STO was tested for its photochemical reactivity under identical illumination conditions. Figure 4(e) shows a decrease in the Ag nanoparticles concentration compared to the 10-nm-thick PZT film on the same substrate (85 μm^{-2} vs 432 μm^{-2}, respectively). Furthermore, EDX analysis of the surface of the 120-nm-thick PZT (Figure 4(f)) showed that the Ag signal is significantly weaker than for the corresponding 10-nm-thick film. This observation is consistent with the assumption that the suppressed photochemical reactivity in thicker PZT is a result of a smaller effect of band-bending and a weaker internal field. This weaker field drives fewer photo-excited carriers to the surface and reduces the rate of photochemical reactions.

In conclusion, we have demonstrated a simple method to control the polarization surface charge and photochemical reactivity of ultrathin PZT thin-films via an appropriate choice of bottom electrode material. The result opens venues

for bottom-up fabrication of templates for multicomponent ferroelectric nano-devices. The imprint control described in this paper could also be further utilized in controlling the ground state of FE-tunneling junctions in resistive switching and for pyroelectric applications.

[1]J. L. Giocondi and G. S. Rohrer, Chem. Mater. **13**(2), 241 (2001).

[2]S. V. Kalinin, D. A. Bonnell, T. Alvarez, X. Lei, Z. Hu, J. H. Ferris, Q. Zhang, and S. Dunn, Nano Lett. **2**(6), 589 (2002).

[3]P. M. Jones, D. E. Gallardo, and S. Dunn, Chem. Mater. **20**(18), 5901 (2008).

[4]S. Dunn, D. Tiwari, P. M. Jones, and D. E. Gallardo, J. Mater. Chem. **17**(42), 4460 (2007).

[5]S. Dunn, P. M. Jones, and D. E. Gallardo, J. Am. Chem. Soc. **129**(28), 8724 (2007).

[6]M. E. Lines and A. M. Glass, *Principles and Applications of Ferroelectrics and Related Materials* (Oxford University Press, 1977).

[7]A. M. Schultz, Y. Zhang, P. A. Salvador, and G. S. Rohrer, ACS Appl. Mater. Interfaces **3**(5), 1562 (2011).

[8]D. Conklin, T. H. Park, S. Nanayakkara, M. J. Therien, and D. A. Bonnell, Adv. Funct. Mater. **21**(24), 4712 (2011).

[9]J. N. Hanson, B. J. Rodriguez, R. J. Nemanich, and A. Gruverman, Nanotechnology **17**(19), 4946 (2006).

[10]S. V. Kalinin, D. A. Bonnell, T. Alvarez, X. Lei, Z. Hu, R. Shao, and J. H. Ferris, Adv. Funct. Mater. **16**(9–10), 795 (2004).

[11]C. W. Tipton, K. Kirchner, R. Godfrey, M. Cardenas, S. Aggarwal, H. Li, and R. Ramesh, Appl. Phys. Lett. **77**(15), 2388 (2000).

[12]J. F. Scott, *Ferroelectric Memories* (Springer, 2000).

[13]N. V. Burbure, P. A. Salvador, and G. S. Rohrer, Chem. Mater. **22**(21), 5831 (2010).

[14]A. Gruverman, O. Auciello, and H. Tokumoto, J. Vac. Sci. Technol. B **14**(2), 602 (1996).

[15]A. L. Roytburd, S. P. Alpay, V. Nagarajan, C. S. Ganpule, and S. Aggarwal, Phys. Rev. Lett. **85**(1), 190 (2000).

[16]V. Nagarajan, S. Prasertchoung, T. Zhao, H. Zheng, J. Ouyang, R. Ramesh, W. Tian, X. Q. Pan, D. M. Kim, C. B. Eom, H. Kohlstedt, and R. Waser, Appl. Phys. Lett. **84**(25), 5225 (2004).

[17]C. L. Jia, N. Valanoor, J. Q. He, L. Houben, T. Zhao, R. Ramesh, K. Urban, and R. Waser, Nature Mater. **6**(1), 64 (2007).

[18]A. L. Kholkin, K. G. Brooks, D. V. Taylor, S. Hiboux, and N. Setter, Integr. Ferroelectr. **22**(1–4), 525 (1998).

[19]L. Tsakalakos and T. Sands, Appl. Phys. Lett. **76**(2), 227 (2000).

[20]S. S. N. Bharadwaja, T. Dechakupt, and S. T. McKinstry, J. Am. Ceram. Soc. **91**(5), 1580 (2008).

[21]N. V. Burbure, P. A. Salvador, and G. S. Rohrer, Chem. Mater. **22**(21), 5823 (2010).

[22]V. M. Fridkin, *Ferroelectric Semiconductors* (Consultans Bureau, 1980).

[23]D. Tiwari, S. Dunn, and Q. Zhang, Mater. Res. Bull. **44**(6), 1219 (2009).

[24]See supplementary material at http://dx.doi.org/10.1063/1.4802885 for additional information including high resolution XRD scans, Ag particle count, and calculations for photon induced temperature rise within the samples.